JOURNAL OF PROPULSION AND POWER
Vol. 14, No. 3, May–June 1998

Analysis of Ar–Cs Magnetohydrodynamics Disk Generator with Strong Interaction

Motoo Ishikawa,* Takuro Shiomi,† and Yoshitaka Inui‡
Kyoto University, Kyoto 606-01, Japan
and
Hiroyuki Yamasaki§
Tokyo Institute of Technology, Tokyo 729-02, Japan

The performance of an Ar–Cs magnetohydrodynamics (MHD) disk generator with strong interaction has been numerically examined and compared with experimental data, leading to the following results: 1) It has been demonstrated for the first time that numerical analyses with the quasi-one-dimensional approximation without an artificial parameter can predict the overall generator performance of a closed-cycle disk MHD generator with strong interaction. The local phenomena of gasdynamics and electrodynamics can be predicted near the designed condition, but some error of prediction is seen under off-designed conditions. 2) It is predicted that instabilities grow near a short-circuit condition. It is demonstrated that the proposed scheme of calculation of ionization is important. 3) The present results suggest that large joule heating is required for the stability of flow, but too much joule heating reduces the generator performance and, therefore, multiloading is suggested for improved generator performance.

Nomenclature

A = duct cross section
B = z component of magnetic field
$E_{()}$ = ( ) component of electric field
$f_{()}$ = ( ) component of friction
h = enthalpy
I = load current
$J_{()}$ = ( ) component of current density
k_B = Boltzmann's constant
$k(p, c)$ = coefficient of ionization rate at level p
$k(p, q)$ = coefficient of excitation or de-excitation rate between levels p and q
m_{Ar} = mass of Ar atoms
m_C = mass of Cs atoms
m_e = electron mass
N = number of levels
n_{Ar} = number density of Ar atoms
n_{co} = total number density of Cs atoms and ions
n_e = electron number density
$n_{i\mathrm{Ar}}$ = number density of Ar ions
n_p = Cs number density at excitation level p
$\dot{n}_p$ = time variation of n_p
p = gas pressure
q = heat loss
R = gas constant
r, θ, z = coordinates
T = gas temperature
t = time
$u_{()}$ = ( ) component of gas velocity
W = radiation loss of electrons
β = Hall parameter
Δt = time step for calculation
δ = collision loss factor of electrons
δ_l = displacement thickness
$\varepsilon_{i\mathrm{Ar}}$ = ionization potential of Ar
$\nu_{()}$ = electron momentum–transfer collision frequency
ν = kinetic molecular viscosity
ρ = gas density
σ = electrical conductivity of gas

Subscripts
r = r component of parameter
θ = θ component of parameter

Received May 13, 1996; revision received June 29, 1997; accepted for publication July 15, 1997.

*Associate Professor, Department of Electrical Engineering, Yoshida-Honmachi, Sakyo-ku.
†Graduate Student, Department of Electrical Engineering, Yoshida-Honmachi, Sakyo-ku.
‡Lecturer, Department of Electrical Engineering, Yoshida-Honmachi, Sakyo-ku.
§Professor, Research Laboratory for Atomic Reactors, O-okayama, Meguro-ku.

Introduction

EXPERIMENTAL studies of closed-cycle magnetohydrodynamics (MHD) power generation, using nonequilibrium plasma and disk generators, were carried out at the Tokyo Institute of Technology, Japan. The working fluid is Ar or He, and experiments were performed at shock-tube facilities and at blowdown facilities with a heat exchanger.

When He is used in shock-tube facilities, the enthalpy extraction ratio is near 40%, indicating that the performance required for commercial-scale generators has been proven for the enthalpy extraction ratio.[1] With the blowdown facilities, performance with He has not been optimized[2] because the majority of effort has been concentrated on the Ar operation.

When Ar is used, an enthalpy extraction ratio near 20% is obtained with the Fuji-I blowdown facilities.[3] With the shock-tube facilities, excellent results were reported by the Research Laboratory for Atomic Reactors, Tokyo Institute of Technology (TIT), Japan,[4] where a disk-type MHD generator was run with Ar seeded with Cs, resulting in a strong MHD interaction.

Research groups of both the TIT and Kyoto University carried out analyses with one-, two-, and three-dimensional approximations,[5–7] revealing the ionization instabilities, the strong interaction between gasdynamics and electrodynamics, and the shock boundary-layer interaction under the MHD conditions. These intensive efforts provided a qualitative understanding of phenomena, but have not been able to predict generator performance with accuracy.

With the present capability of available computers, the one-dimensional analyses are still very important for computations with a wide range of operation parameters. The two-dimensional computation can only be used for a whole generator field with special operating conditions, whereas three-dimensional computation can only be applied for the study of local phenomena. The primary objective of the present report is to examine the experimental data obtained in shock-tube facilities run with Cs-seeded Ar by using the one-dimensional analyses, and one objective is to show the validity and limitation of one-dimensional approximation. Moreover, another important objective is to reveal probable local phenomena, because it is extremely difficult to measure local phenomena within MHD channels in experiments.

Mathematical Model and Assigned Conditions

Gasdynamic Equations

A time-dependent quasi-one-dimensional approximation is used for the gasdynamic equations, where volumetric effects of Cs atoms, ions, and electrons are neglected because their fractions are very small compared with those of Ar atoms. All quantities vary only along the r direction (main flow direction). Flow equations, in cylindrical coordinates, are

Mass continuity equation

$$\frac{\partial}{\partial t}(\rho A) + \frac{\partial}{\partial r}(\rho u_r A) = 0 \tag{1}$$

Momentum equations

$$\rho\frac{\partial u_r}{\partial t} + \rho u_r\frac{\partial u_r}{\partial r} - \frac{\rho u_\theta^2}{r} = -\frac{\partial p}{\partial r} + J_\theta B - f_r \tag{2}$$

$$\rho\frac{\partial u_\theta}{\partial t} + \rho u_\theta\frac{\partial u_\theta}{\partial r} + \frac{\rho u_\theta u_r}{r} = -J_r B - f_\theta \tag{3}$$

Energy equation

$$\rho\frac{\partial}{\partial t}\left(h + \frac{u_r^2 + u_\theta^2}{2}\right) + \rho u_r\frac{\partial}{\partial r}\left(h + \frac{u_r^2 + u_\theta^2}{2}\right) = \frac{\partial p}{\partial t} + J_r E_r - q \tag{4}$$

State equation

$$p = \rho RT = n_{\mathrm{Ar}} k_B T \tag{5}$$

The frictions f_r, f_θ, and the heat loss q are determined from turbulent boundary-layer assumption, where the wall roughness is estimated by the equivalent roughness height of 4.0×10^{-4} m.

The extrapolation of flow quantities is assumed as the exit boundary condition in all cases because the MHD interaction is very strong, although it is not perfect when the flow becomes subsonic.

Boundary-Layer Displacement Thickness

The generator height is modified to take into account the displacement thickness[8] because the generator is small enough that the boundary layer has rather large effects. The distribution of displacement thickness is estimated with no magnetic field and then kept unchanged, even when the MHD interaction is considered

$$\delta_l = \tfrac{1}{8} \times 0.37 r(u_\infty r/\nu)^{-0.2}, \qquad u_\infty = \sqrt{u_r^2 + u_\theta^2} \tag{6}$$

Numerical Scheme

The gasdynamic equations are solved with the MacCormack scheme.[9] A constant mesh system consisting of 191 grids is used along the flow (r) direction. The time step of $\Delta t = 0.1$ μs is used.

Electrodynamical Equations

The basic equations used for the electrodynamics are the steady Maxwell equations and the generalized Ohm's law. The induced magnetic field is neglected because the magnetic Reynolds number is very small under the present conditions

$$\nabla \times E = 0 \tag{7}$$

$$\nabla \cdot J = 0 \tag{8}$$

$$J = \sigma(E + u \times B) - (\beta/\|B\|)(J \times B) \tag{9}$$

$$E_\theta = 0 \tag{10}$$

The quasi-one-dimensional approximation is used for electrodynamics, leading to the following conservation of current density along the generator:

$$J_r = I/A \tag{11}$$

In the computation, I is given and kept constant in the generator.

Nozzle Condition

The open-circuit condition is applied in the nozzle

$$J_r = 0, \qquad E_r = -(u_\theta + \beta u_r)B, \qquad J_\theta = -\sigma u_r B \tag{12}$$

Anode condition

Along the anode the azimuthal component of current density is assumed to be zero

$$J_\theta = 0, \qquad E_r = E_{r1}, \qquad J_r = J_{r1} \tag{13}$$

where E_{r1} and J_{r1} are the values at the exit of anode, which are evaluated with Eqs. (9–11).

Conservation of Ions and Electrons

Conservation of Ion Number Density and Excitation of Cs

Because the ionization process is treated in the nozzle, a detailed model[5] is used for the conservation of ions and electrons, where 10 levels of excited states, including an ionization state, are considered for the ionization of Cs, and a three-body recombination model is used for Ar. About 2000 meshes are incorporated for the calculation of ion conservation, which are much larger than the flow meshes.

Now let n_p be the Cs number density with excitation level p, and then the following continuity equation is obtained:

$$\frac{\partial}{\partial t}(n_p) + \nabla \cdot (n_p u) = \dot{n}_p \qquad (p = 1, 2, 3, \ldots, N) \tag{14}$$

$$\frac{\partial}{\partial t}(n_{i\mathrm{Ar}}) + \nabla \cdot (n_{i\mathrm{Ar}} u) = \dot{n}_{i\mathrm{Ar}} \tag{15}$$

$$n_e = n_{ic} + n_{i\mathrm{Ar}} = \left(n_{co} - \sum_{p=1}^{N} n_p\right) + n_{i\mathrm{Ar}} \tag{16}$$

The time variations of n_p at each excited level are given as

$$\dot{n}_p = -n_p n_e k(p, c) + n_e^2 n_{ic} k(c, p) - n_p n_e \sum_{p \neq q} k(p, q) + n_e \sum_{p \neq q} n_p k(q, p) \tag{17}$$

where $k(p, q)$ is the coefficient of excitation rate from level p to level q, $k(q, p)$ is the coefficient of de-excitation rate from

level q to level p, $k(p, c)$ is the coefficient of ionization rate at level p, and $k(c, p)$ is the coefficient of recombination rate at level p.

Among the 10 levels of Cs considered in the present calculation, excitation rates of the levels 6P to 5D, 7P to 6D, and larger than 8P are very large and, therefore, the levels between 6P and 5D, 7P and 6D, and 8P and ionization are considered to be equilibrium with electron temperature T_e. The validity of the present model was reported in Ref. 5.

Energy Conservation of Electrons

The relaxation process is very fast for the electron energy equation compared with the relaxation process of number densities and, thus, the time-dependent term is neglected, while the equation is solved with the Newton–Raphson method

$$\frac{J_r^2 + J_\theta^2}{\sigma} = \frac{3}{2}\delta k_B n_e m_e (T_e - T)\left(\frac{\nu_{e\mathrm{Ar}}}{m_{\mathrm{Ar}}} + \frac{\nu_{ec}}{m_c} + \frac{\nu_{ei\mathrm{Ar}}}{m_{\mathrm{Ar}}} + \frac{\nu_{eic}}{m_c}\right) + \left(\frac{3}{2}k_B T_e + \varepsilon_{i\mathrm{AR}}\right) + \dot{n}_{i\mathrm{Ar}} + \left(\frac{3}{2}\dot{n}_{ic}k_B T_e - \sum_{p=1}^{N}\dot{n}_p \varepsilon_p\right) + W \tag{18}$$

where δ is assumed to be 2 in the present paper.

Conditions Assigned

The operating parameters used in our calculations are taken from the following experimental data: stagnation temperature at the disk inlet = 2350 K; stagnation pressure at the inlet = 0.245 MPa; wall temperature = 300 K; applied magnetic flux density = 2.7 T (varying along the flow direction); throat radius and height at nozzle = 75 mm and 10.6 mm; anode radius, height, and width = 110, 16.7, and 10 mm; cathode radius and height = 270 and 43.6 mm; and seeding ratio = 8.8×10^{-4}.

Figure 1 depicts the schematic diagram of a disk-type MHD generator and the cylindrical coordinates used in the present paper.

Numerical Accuracy

The sensitivity of calculation results to numerical grid size was investigated. When the number of numerical grids is doubled, the maximum power output is within three decimal points. Also, the structure of disturbance predicted by the present analysis is nearly the same when the grid size is reduced by half.

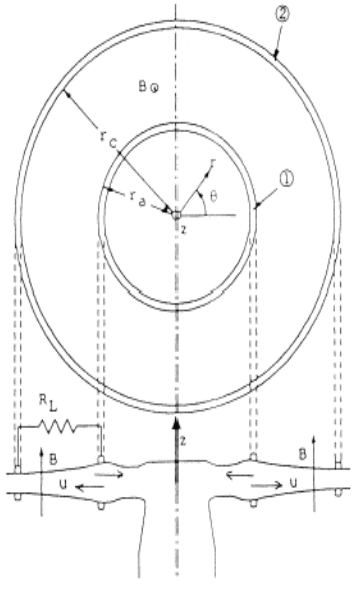

Fig. 1 Schematic diagram of MHD disk channel and coordinates (①, anode and ②, cathode).

Computational Results and Comparison with Experiment

Overall Generator Performance

The strength of interaction is determined by the interaction parameter based on the pressure: interaction parameter = generator length/interaction length, and interaction length = $p/\sigma u B^2$

The interaction parameter based on the stagnation pressure at the entrance is about 1.7, indicating that the interaction of the examined generator is very strong.

The displacement thickness along one wall is about 2 mm at the position of cathode, being about 10% of the generator height of 43.6 mm.

Figure 2 compares the current–voltage characteristics, where the solid line shows the computational result, while the dotted line indicates the experimental result. The agreement is relatively good between the analysis and the experiment as a whole, but the computational results give a better generator performance than the experiment near the short-circuit condition, whereas the calculated power output is lower near the open-circuit condition. In these calculations the ionization of Ar is neglected to reduce the CPU time. It has been found that about a 10% reduction of output voltage results when the ionization of Ar is taken into account and the electron temperature exceeds 7000 K.

Figure 3 shows the enthalpy extraction ratio as a function of loading resistance. Good agreement between the analysis and the experiment is obtained. The maximum enthalpy extraction ratio exceeds 25%, demonstrating that the generator performance required for the commercial use is at least as for the enthalpy extraction.

Figure 4 shows the generator isentropic efficiency as a function of loading resistance. Good agreement between the analysis and the experiment is again obtained. The maximum is-

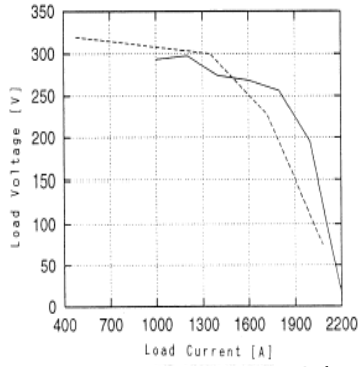

Fig. 2 Comparison of current–voltage characteristics (——, computation and ····, experiment).

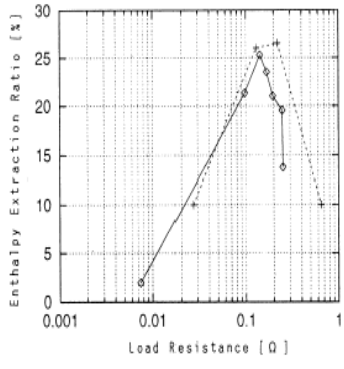

Fig. 3 Relation of enthalpy extraction ratio and loading resistance (——, computation and ····, experiment).

entropic efficiency is near 40%, showing that the generator performance required is not as that needed for the isentropic efficiency, probably because the facilities are too small.

Figures 3 and 4 indicate that the generator shows that its maximum performance occurs at a load resistance of 0.15 Ω. The reason is given as follows: When the loading current is larger, the joule heating is adequate to maintain the full ionization of seed and the MHD interaction becomes weak, whereas while the loading current becomes smaller, the Lorentz force becomes too large and the performance deteriorates.

Figures 2–4 demonstrate that the present analysis can simulate the overall generator performance over a wide range of loading conditions.

Characteristics of Electrodynamics

Figure 5 shows the electric potential distribution along the generator, where the solid and dashed lines indicate the calculated results, and the dotted line with the symbol ◇ indicates the experiment, demonstrating that the local electric field shows good agreement between the computation and experiment. It is also shown that the last quarter of the generator does not operate as a generator. This fact will be discussed in the Instabilities section.

Figure 6 shows the time variation of the electric field distribution, for I = 1200 A, until the steady flowfield is obtained and the initial flowfield is obtained for the loading current of 1400 A. Hereafter, a similar situation is described by I changing from 1400 to 1200 A. Figure 6 shows that the electric field is very smooth in the upstream region, but some disturbance occurs in the downstream region.

Figure 7 depicts the time variation of the Faraday current density distribution with the same variation of I as in Fig. 6. Faraday current shows the same tendency as in Fig. 6, very smooth in the upstream region but unstable in the downstream region. The origin of the electric field and Faraday current disturbance will also be discussed in the Instabilities section.

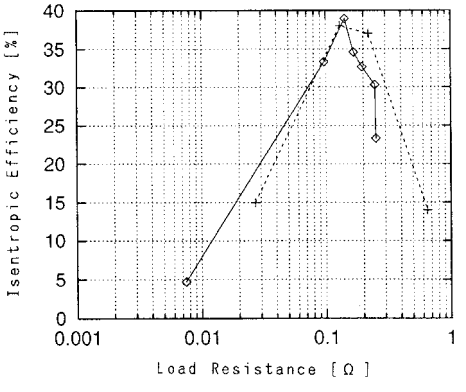

Fig. 4 Relation of isentropic efficiency and loading resistance (——, computation and · · · ·, experiment).

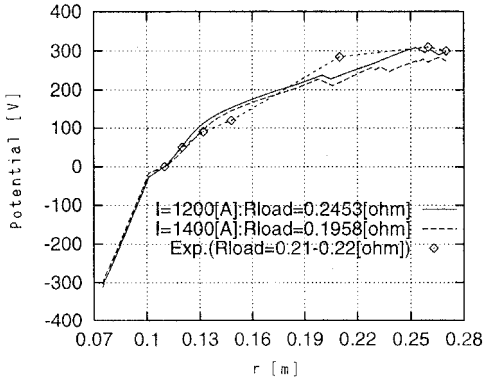

Fig. 5 Comparison of potential distribution (——, computation and · · · ◇ · · ·, experiment).

Characteristics of Gasdynamics

Figure 8 compares the calculated and measured pressure distributions. The symbol ◇ shows the experimental result when the loading resistance is about 0.12–0.13 Ω. The computation assumed that the loading current was 1800 or 2000 A, while the experiment showed that the loading current was 1750 A. The agreement is fairly good, although the computation results in higher pressure at the exit, most likely because the present one-dimensional calculation did not treat the diffuser.

Figure 9 depicts the time variation of the Mach number distribution after I has been changed from 1600 to 1400 A. It has been found that the disturbance grows along the generator, which seems to be related to the electric field distribution shown in Fig. 6 and will be discussed in the next subsection.

Figure 10 shows the time variation of gas temperature distribution after I is changed from 1600 to 1400 A. Note that the disturbance begins to grow from the midpart of the generator.

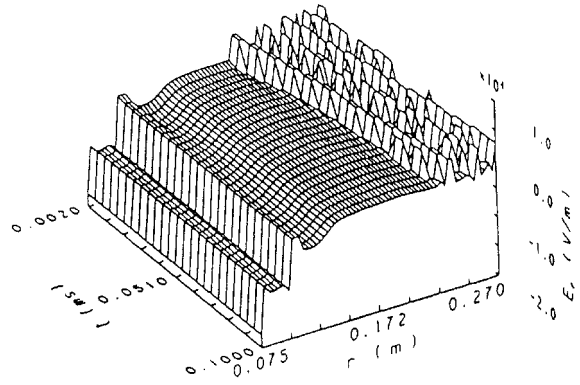

Fig. 6 Variation of distribution of electric field (I = 1400–1200 A).

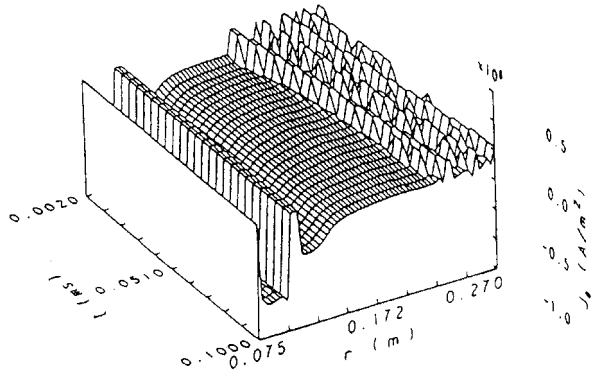

Fig. 7 Variation of distribution of Faraday current density (I = 1400–1200 A).

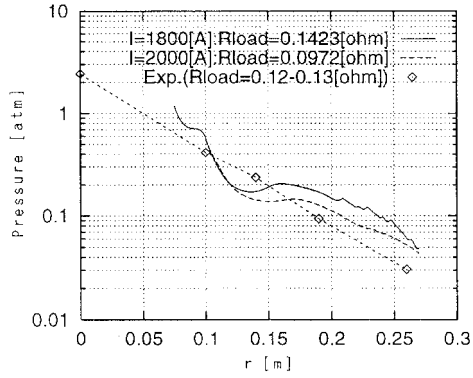

Fig. 8 Comparison of pressure distribution (◇, experiment).

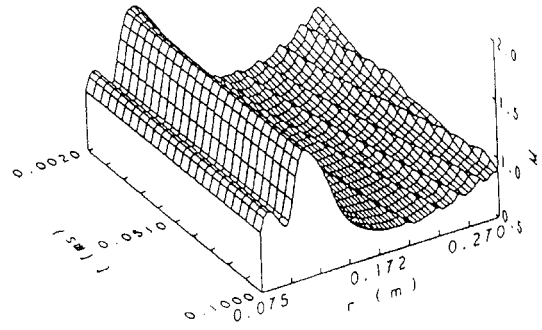

Fig. 9 Variation of distribution of Mach number (I = 1600–1400 A).

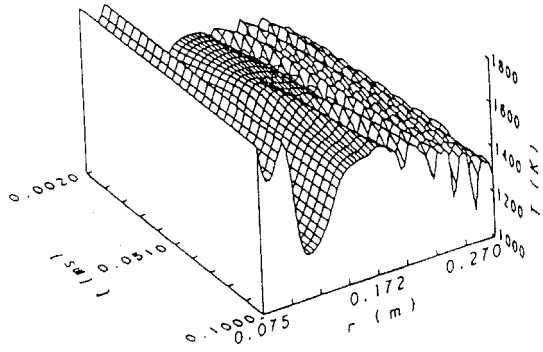

Fig. 10 Variation of distribution of gas temperature (I = 1600–1400 A).

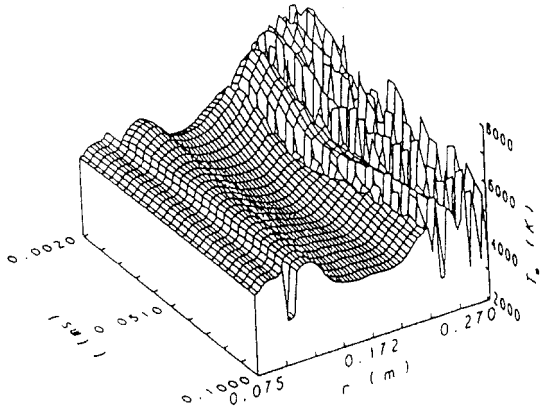

Fig. 11 Variation of distribution of electron temperature (I = 1600–1400 A).

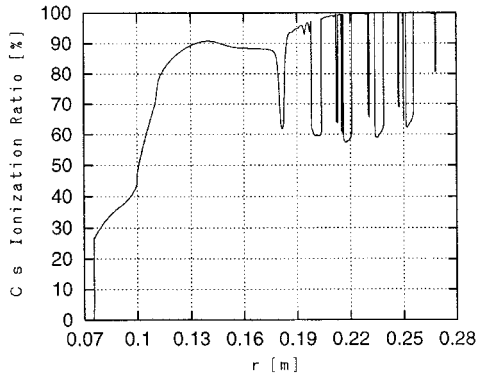

Fig. 12 Distribution of ionization degree of Cs.

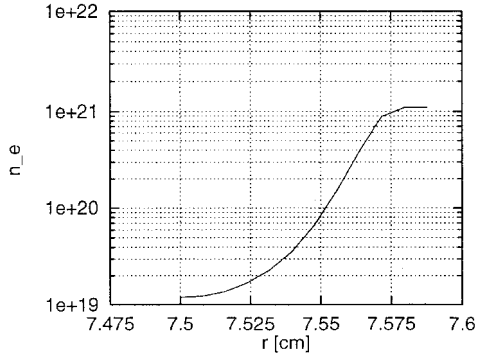

Fig. 13 Detail of ionization process at entrance.

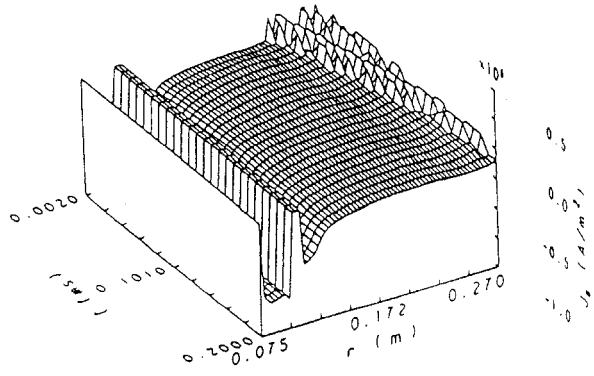

Fig. 14 Variation of distribution of Faraday current density (I = 1200–1000 A).

Instabilities

The computational results show that the flow and electrical disturbances grow along the generator and, thus, in this section we try to examine the nature of the disturbance found in the calculations.

Figure 11 also shows the time of variation of the electron temperature distribution after I changed from 1600 to 1400 A. The disturbance begins to grow from the midsection of the generator and the electron temperature increases to 8000 K, at which point the ionization of Ar begins to have some effect. The experiments also showed the propagation of disturbance along the generator.[4]

Figure 12 depicts the distribution degree of Cs ionization along the generator. The ionization reaches about 90% at the beginning of the generator and then becomes unstable. The instability begins when the cesium approaches the state of full ionization and the magnitude in the fluctuation of ionization is very large; the degree of ionization fluctuates between 60 and 100% at the latter half of generator.

Figure 13 shows details of the ionization process at the entrance region of nozzle, where the inlet ionization is assumed to be equilibrium with 2000 K. Twelve meshes are incorporated for only 1 mm, and very rapid ionization is seen along the nozzle from about 10^{19} to about 10^{21} m^{-3}.

The relationship between the instability and loading current is then examined. Figure 14 shows the time variation of the Faraday current density distribution after I changes from 1200 to 1000 A, indicating that when the loading current is 1200 A, the performance remains unstable, but when the loading current is lowered to 1000 A, the performance becomes stable.

Figure 15 depicts the time variation of the Mach number distribution, where I changes from 1000 to 800 A, showing that the flow is always stable.

We now discuss the reason why the disturbance tends to grow at the downstream part of the generator. At the upstream part, the radial electric field is always adequate because the velocity is large enough and the ionization is made adequate along the nozzle, and the resulting large joule heating maintains almost full ionization of Cs; however, at the downstream part of the disk generator, the electric field is reduced because

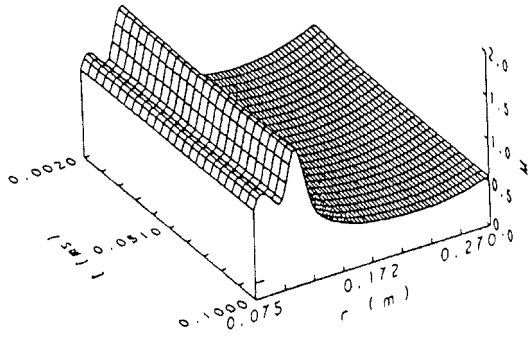

Fig. 15 Variation of distribution of Mach number (I = 1000–800 A).

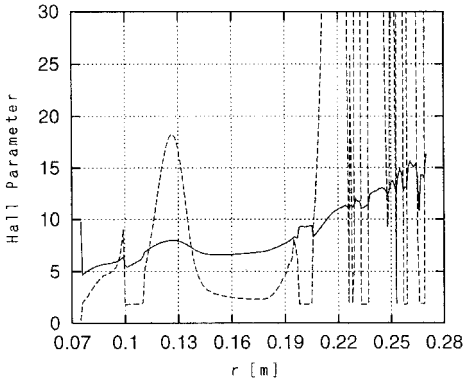

Fig. 16 Distribution of Hall parameter and critical Hall parameter (I = 1400 A).

of local load mismatching. Full ionization of Cs becomes too difficult to maintain (Fig. 12), when the loading current is increased. These computational results indicate that the generator behaves in an unstable manner when operated near short-circuit conditions, whereas it becomes stable when operated near open-circuit conditions, revealing that when the joule heating is adequate, the generator is stable, and when the joule heating is not adequate, the generator becomes unstable. In addition, if the disturbance rises, the electron temperature over 8000 K spikes, the ionization of Ar is initiated, and the disturbance is enhanced (Fig. 11).

Finally, conventional ionization instabilities are examined in terms of the conventional critical Hall parameter. Figure 16 depicts the distribution of the Hall parameter and the critical Hall parameter along the generator when the loading current is 1400 A. The critical Hall parameter is estimated with the Saha equilibrium between the electron number density and the electron temperature, neglecting the ionization of Ar because many calculations here are carried out without Ar ionization. Along the first half of the generator the Hall parameter is about two times higher than the critical Hall parameter, and then the critical Hall parameter becomes much higher than the Hall parameter, fluctuating as the instabilities increase. As seen in the numerical results, the generator is stable in the first half of the generator, whereas the generator becomes unstable in the second half of the generator, showing that the simple linear analysis cannot predict the stability. This is probably why the simple linear analysis depends on the instant Saha equilibrium, but our model is much more complicated and the convection effect is very large and, therefore, kinetic effects are dominant within the MHD generator with the strong interaction. Additional studies are required that include r-θ two-dimensional analysis.

Suggestions for Improved Performance

The present numerical results revealed that large joule heating is required for the stability of plasma and flow itself, but local load matching sometimes becomes impossible. The experiment yielded its best performance with the existence of partial instability within the generator. We then suggest that the load be divided and, thus, both the plasma stability and local load matching can be satisfied simultaneously. This proposal will be explored with the validated present code.

Concluding Remarks

1) It has been demonstrated for the first time that numerical analyses with the quasi-one-dimensional approximation without any artificial parameter can predict the overall generator performance of a closed-cycle disk MHD generator with a strong interaction operated with Ar–Cs. The local phenomena of gasdynamics and electrodynamics can be predicted well with the present one-dimensional analysis near the designed condition, but some error of prediction is seen with off-designed conditions.

2) It is predicted that instabilities grow near the short-circuit condition and the phenomena somewhat agree with the experiment. The detailed study is required for the instabilities. It is demonstrated that the proposed scheme of calculation of ionization is important.

3) The present result suggests that extensive joule heating is required for stability, but joule heating that is too extensive reduces the generator performance and, therefore, multiloading is suggested for improvement of the generator.

Acknowledgments

A part of the present computation was carried out on the computer of The National Institute of Nuclear Fusion. This study was supported in part by the Kansai Electric Company.

References

[1]Okamura, T., Harada, N., Kabashima, S., Yoshikawa, K., Yamasaki, H., Suekane, T., Tsuji, K., Okuno, Y., Shioda, S., Hasegawa, Y., Matsutani, K., Ishimura, M., Dozono, Y., and Ikeda, S., "Review and New Results of High Enthalpy Extraction Experiments at TIT," *Proceedings of the 32nd Symposium on Engineering Aspects of MHD, Session 11*, Pittsburgh Energy Technology Center, Pittsburgh, PA, 1994.

[2]Harada, N., Suekane, T., Tsunoda, K., Yoshikawa, K., Yamasaki, H., Kabashima, S., Shioda, S., Hasegawa, Y., Ishimura, M., Dozono, Y., and Ikeda, S., "Results of Fuji-1 Power Experiment Driven by He," *Proceedings of the 29th Symposium on Engineering Aspects of MHD, VIII.3* (New Orleans, LA), 1991, pp. 1–9.

[3]Okuno, Y., Okamura, T., Yoshikawa, K., Suekane, T., Ohgaki, K., Tsuji, K., Kabashima, S., Shioda, S., Yamasaki, H., Hasegawa, Y., Harada, N., Matsutani, K., Tezuka, M., Dozono, Y., and Ikeda, S., "Recent Activities on CCMHD Power Generation Studies with Fuji-1 Blow-Down Facility," *Proceedings of the 33rd Symposium on Engineering Aspects of MHD, II.1* (Tullahoma, TN), 1995.

[4]Tsuji, K., Niwa, Y., Kaneko, T., Yamashita, A., Tsutsui, M., Okubo, M., and Yamasaki, H., "Highest Enthalpy Extraction from CCMHD Disk Generator with Cesium Seeded Argon," *Proceedings of the 32nd Symposium on Engineering Aspects of MHD, Session 11*, Pittsburgh Energy Technology Center, Pittsburgh, PA, 1994.

[5]Inui, Y., Noguchi, H., Ishikawa, M., and Umoto, J., "New Calculation Method of Electron Density of Nonequilibrium MHD Plasma Considering Excited States of Seed Atom," *Proceedings of the 32nd Symposium on Engineering Aspects of MHD, Session 4*, Pittsburgh Energy Technology Center, Pittsburgh, PA, 1994.

[6]Kabashima, S., Kobayashi, H., Maeda, T., Yasui, K., and Suekane, T., "Numerical Simulation of MHD Flow in the Disk MHD Generator," *Proceedings of 17th Symposium on Efficient Use of Energy and Direct Electrical Power Generation, 5.1*, Hokkaido Univ., Sapporo, Japan, 1995, pp. 275–284.

[7]Irino, M., Osada, I., Omura, N., Hashizaki, K., Horioka, T., Nishikawa, H., Kabashima, S., Okamura, T., Yoshikawa, K., Yamasaki, H., and Shioda, S., "3-D Calculation of Fuji-I Disk Type MHD Generator," *Proceedings of the 17th Symposium on Efficient Use of Energy and Direct Electrical Power Generation, 5.3*, Hokkaido Univ., Sapporo, Japan, 1995, pp. 295–309.

[8]Schlichting, H., *Boundary-Layer Theory*, 6th ed., McGraw–Hill, New York, 1968, pp. 598, 599.

[9]MacCormack, R. W., "The Effect of Viscosity in Hypervelocity Impact Cratering," AIAA Paper 69-354, May 1969.